

Fully Boron-Sheet-Based Field Effect Transistors from First-Principles: Inverse Design of Semiconducting Boron Sheets

Yi-Lin Zhang, Ji-Hui Yang,* Hongjun Xiang, and Xin-Gao Gong*



Cite This: *J. Phys. Chem. Lett.* 2021, 12, 576–584



Read Online

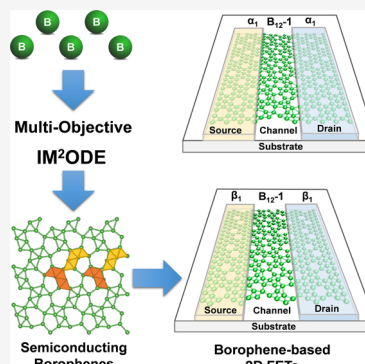
ACCESS |

Metrics & More

Article Recommendations

Supporting Information

ABSTRACT: High-performance two-dimensional (2D) field effect transistors (FETs) have a broad application prospect in future electronic devices. The lack of an ideal material system, however, hinders the breakthrough of 2D FETs. Recently, phase engineering offers a promising solution, but it requires both semiconducting and metallic phases of materials. Here we suggest borophenes as ideal systems for 2D FETs by theoretically searching semiconducting phases. Using multiobjective differential optimization algorithms implemented in the IM²ODE package and the first-principles calculations, we have successfully identified 16 new semiconducting borophenes. Among them, the B₁₂-1 borophene is the most stable semiconducting phase, whose total energy is lower than any other known semiconducting borophenes. By considering not only the band alignments but also the lattice matches between semiconducting and metallic borophenes, we then have theoretically proposed several device models of fully boron-sheet-based 2D FETs. Our work provides beneficial ideas and attempts for discovering novel borophene-based 2D FETs.



The exfoliation of graphene¹ has stimulated wide and profound research of two-dimensional (2D) materials. With the decrease in dimension, 2D materials with various properties are drawing increasing interest because of their great promise in nanoelectronics,^{2,3} plasmonics,^{4,5} photovoltaics,^{6,7} and nanocatalysts^{8,9} as well. Especially, 2D semiconductors

show superior properties for short-channel field effect transistors (FETs) because electrons in 2D materials are limited in the naturally atomically thin channels, thus suppressing current leakage and allowing uniform manipulation of carriers by the gate voltage.¹⁰ With the size of traditional FETs based on 3D semiconductors approaching physical limits and Moore's Law starting to falter due to short-channel effects, FETs based on 2D materials are expected to complement existing technologies and show superiority in more and more applications.

Generally speaking, the performance of FETs is determined not only by the semiconducting channels but also by contact properties between metal electrodes and semiconductor channels. For the former, 2D semiconductors with higher carrier mobility and sizable bandgaps are preferred to ensure high switching speeds and on/off ratios. While current research mainly focuses on the transition metal dichalcogenides (TMDs) and few-layer black phosphorus,^{11,12} they have some other issues like low carrier mobility¹³ or instability. Therefore, new 2D semiconductor channel materials for FETs are still being sought. For the latter, the contact resistance between metal electrodes and semiconductor channels needs to be low enough to form Ohmic contacts in order to reach the

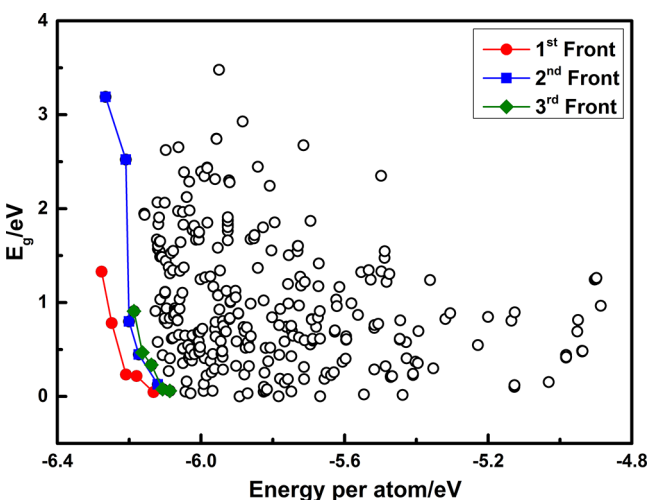


Figure 1. Multiobjective optimization of B₁₂ borophenes in one trial search. The objective functions are the total energy per atom and the bandgap. Black hollow dots represent all candidate structures in the solution space. Red dots represent the 1st Pareto solution set, which fit most to both objective functions. Blue and green dots represent the 2nd and the 3rd Pareto solution sets.

Received: November 7, 2020

Accepted: December 18, 2020

Published: December 31, 2020

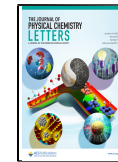


Table 1. Total Energies, Formation Energies, and Band Gaps of Our Identified Semiconducting Boron Sheets in Comparison with Those Values of Metallic Borophenes and Previously Reported Semiconducting Borophene^a

borophenes	energy per atom E_{PBE}/eV	energy per atom $E_{\text{HSE06}}/\text{eV}$	formation energy per atom E_f/eV	band gap $E_{\text{g-PBE}}/\text{eV}$	band gap $E_{\text{g-HSE06}}/\text{eV}$
α_1 (ref 22)	-6.305	-6.941	0.374		
β_1 (ref 22)	-6.292	-6.928	0.387		
$B_{1/8}$ (ref 18)	-6.313	-6.951	0.366		
$B_{2/15}$ (ref 18)	-6.309	-6.948	0.370		
χ_3 (ref 20)	-6.269	-6.896	0.410		
$B_{1/6}$ (ref 20)	-6.257	-6.901	0.422		
β_s^3 (ref 23)	-6.202	-6.830	0.477	0.420	0.633
B_{8-1}	-6.207	-6.857	0.472	0.210	0.591
B_{8-2}	-6.101	-6.747	0.579	0.053	0.552
B_{8-3}	-6.090	-6.734	0.590	0.467	1.006
B_{10-1}	-6.160	-6.797	0.519	0.301	0.707
B_{10-2}	-6.140	-6.796	0.539	0.589	0.932
B_{10-3}	-6.112	-6.747	0.567	0.410	0.710
B_{10-4}	-6.111	-6.756	0.568	0.386	0.772
B_{10-5}	-6.001	-6.648	0.678	1.102	1.765
B_{12-1}	-6.208	-6.860	0.472	0.560	0.880
B_{12-2}	-6.186	-6.832	0.493	0.539	0.776
B_{12-3}	-6.163	-6.823	0.516	0.157	0.538
B_{12-4}	-6.129	-6.771	0.550	0.092	0.347
B_{12-5}	-6.083	-6.726	0.596	0.447	0.843
B_{12-6}	-6.083	-6.722	0.597	0.237	0.492
B_{12-7}	-6.074	-6.728	0.605	1.212	1.879
B_{12-8}	-6.045	-6.674	0.634	0.170	0.290
B_{12-9}	-6.041	-6.678	0.638	1.120	1.629

^aThe formation energy is defined as the difference of energy per atom between borophene and stable bulk B_{12} . The relatively most stable phases identified by us are highlighted in bold.

ballistic limit for high and efficient logic switching.¹⁰ So far, this is quite challenging because Schottky barriers commonly exist between 2D channels and metallic electrodes. In order to reduce or eliminate Schottky barriers, molecule doped multilayers or metal electrodes with appropriate work functions have been used as contacts¹⁴ but the success is quite limited to a few cases. Recently, phase engineering has shown great potential in reducing the contact resistance between electrode and 2D channel by forming their lateral heterostructures. For example, by using metallic 1T-MoS₂ as the electrode, contact resistance in semiconducting 2H-MoS₂ based FETs is unexpectedly decreased mainly due to the atomically sharp interface and lower Schottky barrier between the phases.¹⁵ In addition, phase engineering in MoTe₂ by laser irradiation has been shown to fabricate Ohmic contacts.¹⁶ Despite phase engineering strategy offering a successful route for building 2D FETs with low contact resistance, it requires a 2D material to have both semiconducting and metallic phases to form lateral heterostructures with sharp interfaces. Such 2D systems with metallic phase as electrodes and the semiconducting phase as channel materials, therefore, are the most ideal systems for 2D FETs, which are strongly desired.

Among known 2D systems, the atomic monolayer composed of boron atoms, also known as borophene, has very rich polymorphism, thus providing great potential for the above-mentioned phase-engineering 2D FETs. Theoretically, by just focusing on the energetic stability, various boron sheets have

been systematically predicted.^{17–29} Stimulated by these pioneer theoretical works, some of the predicted structures have been successfully synthesized on metal substrates.^{30–33} However, most of the boron sheets are concluded to be metallic except for the α' -boron sheet.²⁷ These metallic borophenes have been proposed to act as electrodes of FET devices. However, in these systems, the Schottky barriers commonly exist^{34–37} in vertical junctions between metallic borophenes and other 2D semiconductors. Recently, Xu et al.³⁸ proposed a family of semiconducting borophenes by considering the connection of networks of hexagonal vacancies. Ipek et al.³⁹ also found that vacancy-free polymorph of borophene with the triangle lattice is semiconducting due to Peierls distortion. Hou et al. reported the first experimental breakthrough of ultrastable and semiconducting hydrogenated borophene.^{40,41} As the atomic structures of borophene are sensitive to growth conditions and types of the substrates, more semiconducting phases of borophene are expected to be discovered. Stimulated by the success of phase engineering in fabricating 2D FET devices, it will be of great interest to explore the potential of using metallic borophenes as electrodes and semiconducting borophenes as channels to form lateral-junction based 2D FETs.

In this work, by considering not only the total energies but also the electronic properties, we design semiconducting boron monolayers on the basis of multiobjective differential optimization algorithms implemented in our self-developed IM²ODE package. The acw-borophene in ref 39 is automatically identified using our method. What is more, we identify 16 other structures that are both semiconducting and dynamically stable without imaginary frequencies in their phonon spectra. Among them, the B_{12-1} structure is the most stable semiconducting borophene energetically, even compared to previously proposed acw- and β_s^3 -borophenes, thus demonstrating the advantages of our multiobjective structure searching method. In addition, we also find B_{12-2} structure has a very relatively low total energy and is more stable than β_s^3 -borophene according to our HSE06 calculations. Besides, we find the band gaps of semiconducting borophenes can cover a large range from 0.3 to 1.9 eV, providing potentials for various applications. We then consider the band alignments between our designed semiconducting borophenes and the known metallic borophenes to see if they can form Ohmic contacts. Our calculations show that acw-borophene can form a good contact with synthesized χ_3 and $B_{1/6}$ borophenes, while B_{12-1} and B_{12-2} borophene can form good contacts with metallic α_1 and β_1 borophenes. With both semiconducting and metallic phases of borophenes in hand, we then theoretically propose several device models of fully boron-sheet-based 2D FETs with Ohmic contacts by choosing appropriate electrodes and channels with suitable band alignments and lattices. For example, using metallic α_1 borophene as the electrodes of source and drain and using B_{12-1} borophene as the semiconducting channel, n-type FET devices can be formed without Schottky barriers. Our work may open up a new direction of 2D FET devices and can be applied to help the design of 2D FETs with Ohmic contacts based on phase engineering.

DE Based Global Optimization Method for 2D Material Design. We use our IM²ODE package⁴² to perform multi-objective structure search. In the family of global optimization algorithms, the differential evolution method is developed to solve the global optimization problem of continuous

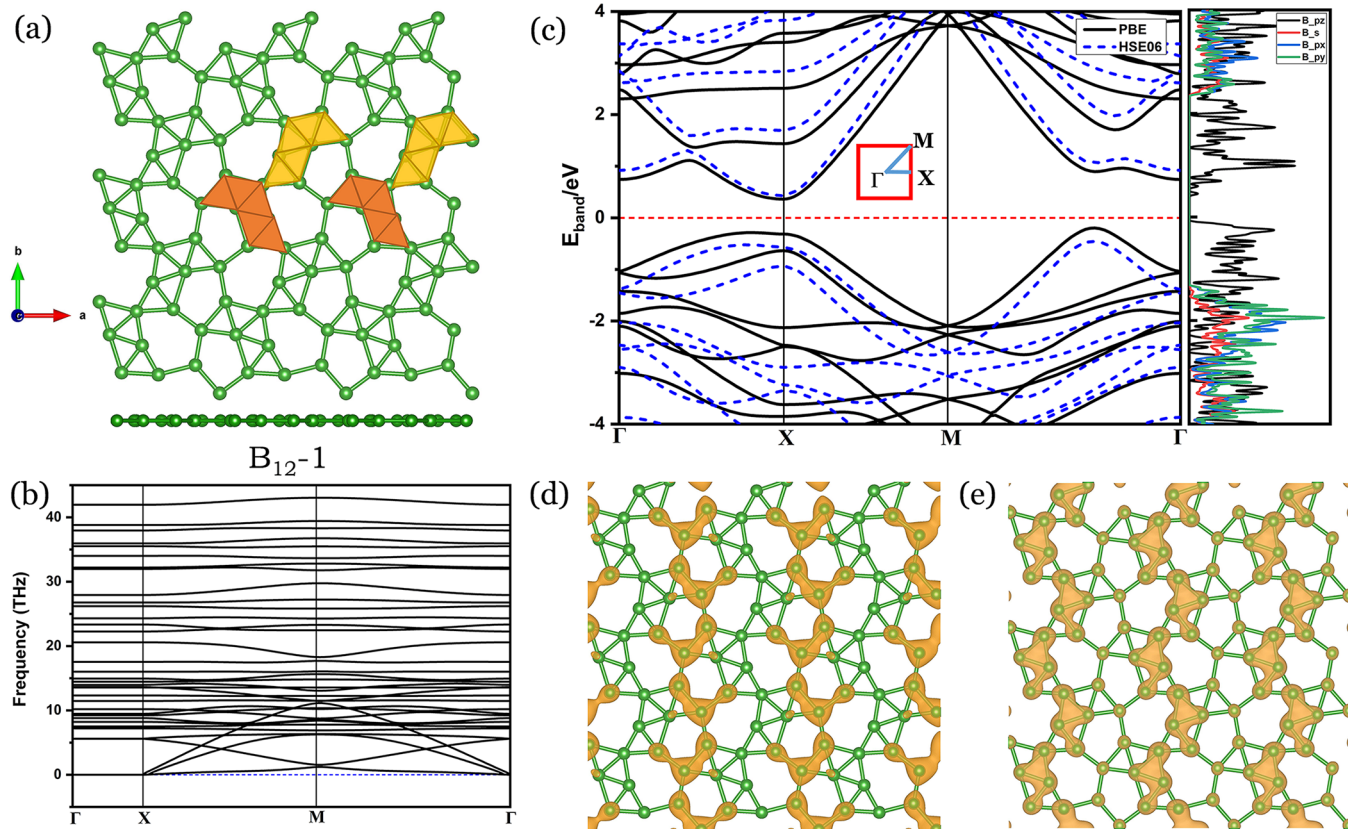


Figure 2. Atomic structure and electronic structure of the most stable semiconducting B₁₂-1 borophene. (a) Structure of B₁₂-1 borophene and basic motifs of five-boron-triangles. (b) Phonon spectrum of B₁₂-1 borophene. (c) Band structure and orbital-resolved DOS of B₁₂-1 borophene. Partial charge densities of (d) the VBM and (e) the CBM of B₁₂-1 borophene.

variables.⁴³ Quite often there is more than one objective function to be optimized; thus, the multiobjective differential evolution (MODE) method is applied. The multiobjective optimization is often written as

$$\min Z(x) = [z_1(x), z_2(x), \dots, z_k(x)]$$

where x is the decision variable and $z_i(x)$ are several objective functions. The very set of x that makes multiobjective function $Z(x)$ meet the optimization demand is called the Pareto solution set. In MODE algorithm, every candidate of a solution is marked as a D -dimensional vector $\mathbf{p}_{i,G}$ that is involved in three steps of MODE progress: mutation, crossover, and selection. For the i th target vector $\mathbf{p}_{i,G}$, the mutant vector $\mathbf{u}_{i,G+1}$ is generated by the mutation operation:

$$\mathbf{u}_{i,G+1} = \begin{cases} \mathbf{p}_i + F_D(\mathbf{p}_{r_1} - \mathbf{p}_{r_2}) & \text{if } \mathbf{p}_i \text{ in the Pareto optimal solution set} \\ \gamma \mathbf{p}_{\text{best}} + (1 - \gamma) \mathbf{p}_{i,G} \\ + F_D(\mathbf{p}_{r_1} - \mathbf{p}_{r_2}) & \text{others} \end{cases}$$

where G denotes the generation and \mathbf{p}_{best} denotes the best solution in present generation. Parameter γ controls the random ratio in mutation. \mathbf{p}_{r_1} and \mathbf{p}_{r_2} are randomly chosen from present generation, $r_1, r_2 \in \{1, 2, \dots, N\}$ and $r_1 \neq r_2 \neq i \neq \text{best}$. Parameter F_D manipulates the differential vector. The crossover step mixes the mutant vector with the parental vector from previous generation to create the trial vector for the next generation $\mathbf{p}_{i,G+1} = (\mathbf{p}_{1i,G+1}, \mathbf{p}_{2i,G+1}, \dots, \mathbf{p}_{Di,G+1})$ by the following scheme:

$$\mathbf{p}_{ji,G+1} = \begin{cases} \mathbf{u}_{ji,G+1} & \text{if } r(j) \leq \text{CR or } j = rn(i) \\ \mathbf{p}_{ji,G} & \text{if } r(j) > \text{CR and } j \neq rn(i) \end{cases}$$

where CR is a constant manually set from 0 to 1 to control the probability of crossover and $r(j)$ is randomly generated within the same range [0,1]. The greedy principle is applied in the selection step of MODE, that is, the trial vector $\mathbf{p}_{i,G+1}$ is compared with target vector $\mathbf{p}_{i,G}$ in the present generation and $\mathbf{p}_{i,G+1}$ will not be accepted unless it is better than $\mathbf{p}_{i,G}$. In our work, the three parameters are set as $\gamma = 0.2$, $F_D = 0.2$, and $\text{CR} = 1.0$. In the case of structure search, the solution sets are atom coordinates.⁴⁴ To improve the searching efficiency, a symmetry constraint is planted in the generation of structures in every MODE step. For each structure that eventually generated after one step, the structural local minimum is guaranteed by relaxation under first-principles calculations. The objective functions are the total energy of borophene E_{total} and the band gap E_g . The optimization targets are as follows:

$$\min Z_1 = E_{\text{total}}$$

$$\max Z_2 = E_g$$

We limit the number of boron atoms in one cell to be 4/6/8/10/12 during the search considering our computational cost. For each case, we repeat our structure search by at least 5 times in order to avoid possible traps of local minimum. Thirty structures in each generation and 30 generations are used in the differential evolution. In each generation, 60% of the structures are generated by the differential evolution algorithm

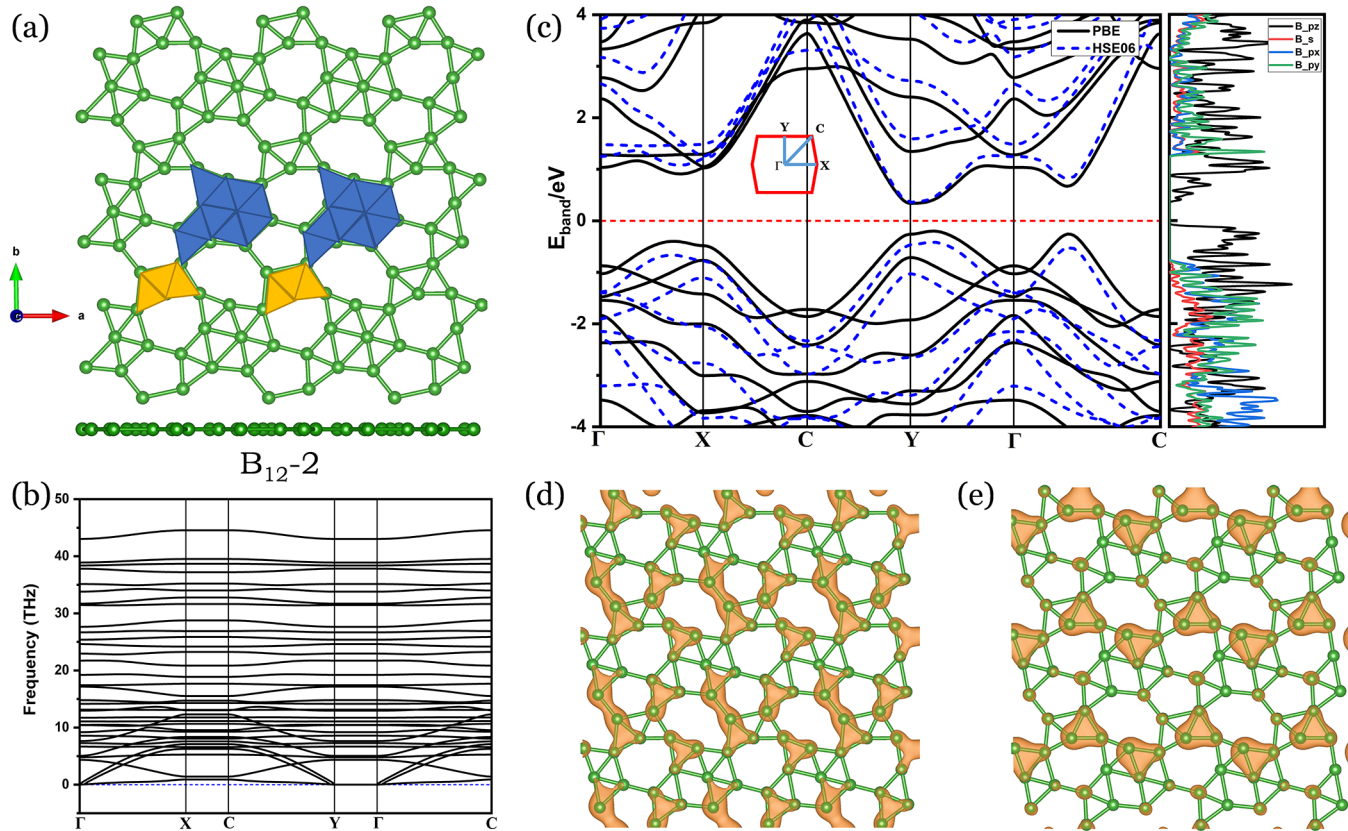


Figure 3. Atomic structure and electronic structure of semiconducting B₁₂-2 borophene. (a) Structure of B₁₂-2 borophene and basic motifs of nine and three boron triangles. (b) Phonon spectrum of B₁₂-2 borophene. (c) Band structure and orbital-resolved DOS of B₁₂-2 borophene. Partial charge densities of (d) the VBM and (e) the CBM of B₁₂-2 borophene.

and the other 40% are randomly generated as mutation seeds. One trial search result is given in Figure 1 to show how we use the Pareto front to choose the best structures that satisfy both the low total energy and finite band gap.

First-Principles Calculation Methods. The structure relaxations and total energy calculations are performed using first-principles methods based on density functional theory (DFT) implemented in the VASP package.⁴⁵ The Projected Augmented Wave (PAW)⁴⁶ method is used for ion-electron interaction and the PBE functional from Generalized Gradient Approximation (GGA)⁴⁷ is used for the exchange correlation. The plane wave cutoff energy is set to be 550 eV. For the Brillouin integration, the Γ -centered Monkhorst–Pack grid sampling method is used⁴⁸ and the sampling k-point spacing in the reciprocal space is less than $2\pi \times 0.04 \text{ \AA}^{-1}$. The electronic structures are further calculated using the HSE06 functional with 25% of Hartree-Fock exchange to give a better evaluation of the bandgap values. The band alignments among different borophenes are determined by aligning the vacuum levels.

By carrying out multiobjective optimizations of both total energy and band gap with the help of first-principles calculations, we find 46 candidates of semiconducting boron monolayers. By further checking their dynamic stabilities through phonon calculations, we finally identify 17 stable semiconducting borophenes. Table 1 lists the total energies, formation energies, and bandgaps of these boron semiconductors in comparison with the data of metallic borophenes and previously reported semiconducting borophene. The formation energy E_f per atom is defined as follows:

$$E_f = \frac{E_{\text{borophene}} - E_{\text{bulk-B}_{12}}}{12}$$

where $E_{\text{borophene}}$ and $E_{\text{bulk-B}_{12}}$ are the calculated total energies of borophene and pure bulk B₁₂, respectively. As we can see, the total energies per atom of our identified boron sheets are very close to the values of previous boron phases.

Among our identified semiconducting borophenes, we find that the B₈-1 phase is actually the acw-borophene reported in ref 39, indicating that our algorithm can successfully predict structures with targeted electronic properties. However, the β_s^3 borophene is not identified during the search, in agreement with the statement in the ref 38. One of the possible reasons is that the β_s^3 structure is very close to the metallic phases of borophene in the potential energy landscape and thus it can easily slip to the more energetically stable metallic borophenes. Despite this, we find that B₈-1 (acw-borophene), B₁₂-1, and B₁₂-2 have lower energies than the artificially built β_s^3 structure according to our HSE06 calculations. In the following, we discuss the properties of structures and electronic structures of our identified semiconducting borophenes.

First, we discuss the properties of B₁₂-1 borophene. As far as we know, the B₁₂-1 structure, first identified by us, is the most stable semiconducting phase of borophene. Its total energy is 1 meV/atom (3 meV/atom) and 6 meV/atom (30 meV/atom) lower than the previously reported acw-borophene (B₈-1) and β_s^3 borophene, respectively, according to our PBE (HSE06) calculations. The structure of B₁₂-1 borophene is shown in Figure 2a. As can be seen, the structure is completely planar in a 2D atomic layer. The basic motifs of this structure are two

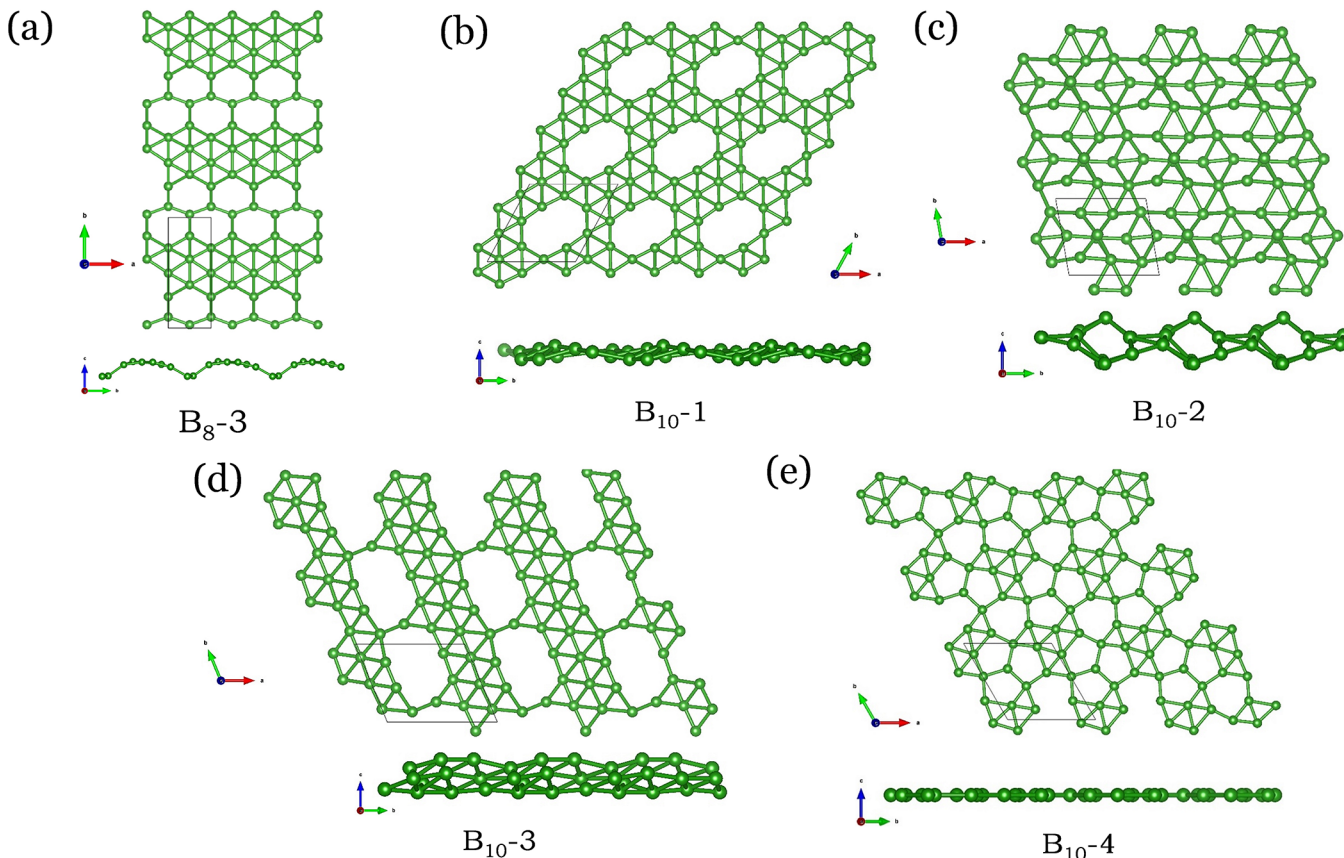


Figure 4. Atomic structures of candidate semiconducting borophenes that could be seen as reconstruction patterns after creating certain boron vacancies from the vacancy-free boron triangle lattices. Top and side views of (a) $B_8\text{-}3$, (b) $B_{10}\text{-}1$, (c) $B_{10}\text{-}2$, (d) $B_{10}\text{-}3$, and (e) $B_{10}\text{-}4$ borophenes.

kinds of five boron triangles, in which four triangles are arranged linearly and one triangle is attached on the right or left side. The two kinds of motifs are connected through hollow pentagons and hexagons by sharing vertices but no edges. This structure might be obtained using the basic motifs as growing pieces. The phonon spectrum of $B_{12}\text{-}1$ borophene is shown in Figure 2b. The absence of imaginary frequencies indicates that it can be dynamically stable in the free-standing form. We also perform molecular dynamics at $T = 300$ K and find the structure is stable (see Figure S1a in the Supporting Information).

The band structure of $B_{12}\text{-}1$ borophene calculated by PBE and HSE06 functionals are given in Figure 2c. The band gap is indirect with the valence band maximum (VBM) along the $M\text{-}\Gamma$ line and the conduction band minimum (CBM) at the X point and its value is 0.88 eV. Densities of states (DOS) show that the p_z orbital dominates around the band edges. Partial charge density in Figure 2d,e shows that the VBM is mainly distributed on those boron atoms with four neighbors and the CBM is mainly distributed on those boron atoms with five neighbors. Interestingly, the two five-coordinated boron atoms are shared by the two kinds of motifs and form one bond, which is surrounded by the four-coordinated boron atoms. Such an arrangement may lead to the suitable filling of p-orbitals of boron atoms and contributes to the gap opening.

The second most stable semiconducting borophene identified using our algorithms is $B_8\text{-}1$, which is the acw-borophene reported in ref 39. As previously discussed by ref 39, this structure is free of boron vacancies. It can be stabilized due to Peierls distortion. Note that the structure keeps the

triangle lattice and thus can be easily patched to the metallic borophenes. We will discuss this point later.

The third most stable semiconducting borophene is $B_{12}\text{-}2$ borophene. According to our HSE06 results, the total energy of $B_{12}\text{-}2$ borophene is 2 meV/atom lower than the artificially built β_s^3 phase. Similar to the $B_{12}\text{-}1$ phase, $B_{12}\text{-}2$ borophene is also planar, as seen in Figure 3a. Its structure can be seen as composing one motif of nine triangles and the other motif of three triangles. These motifs are connected by hollow pentagons, hexagons, and heptagons. The phonon spectrum in Figure 3b and molecular dynamics calculations in the Figure S1b support the dynamic stability and thermodynamic stability of $B_{12}\text{-}2$ borophene, respectively.

Figure 3c shows the band structure of $B_{12}\text{-}2$ borophene calculated by PBE and HSE06 functionals. With the VBM at the Y point and the CBM along the $Y\text{-}\Gamma$ line, $B_{12}\text{-}2$ borophene has an indirect bandgap of 0.78 eV. Similar to the $B_{12}\text{-}1$ phase, the band edges of $B_{12}\text{-}2$ borophene are also dominated by p_z orbitals, as seen in the DOS. Partial charge densities in Figure 3d,e show that the VBM and CBM states are spatially distributed on different boron atoms, which are also similar to $B_{12}\text{-}1$. Such band character is expected to be useful for electron–hole separation.

We note that both $B_{12}\text{-}1$ and $B_{12}\text{-}2$ borophenes can be effectively seen as reconstruction patterns after creating certain boron vacancies from the vacancy-free boron triangle lattices. So, in principle, if vacancy-free boron triangle lattices can be made, both the metallic and semiconducting phases of borophenes can be fabricated by selectively knocking out boron atoms. In fact, several other semiconducting borophenes

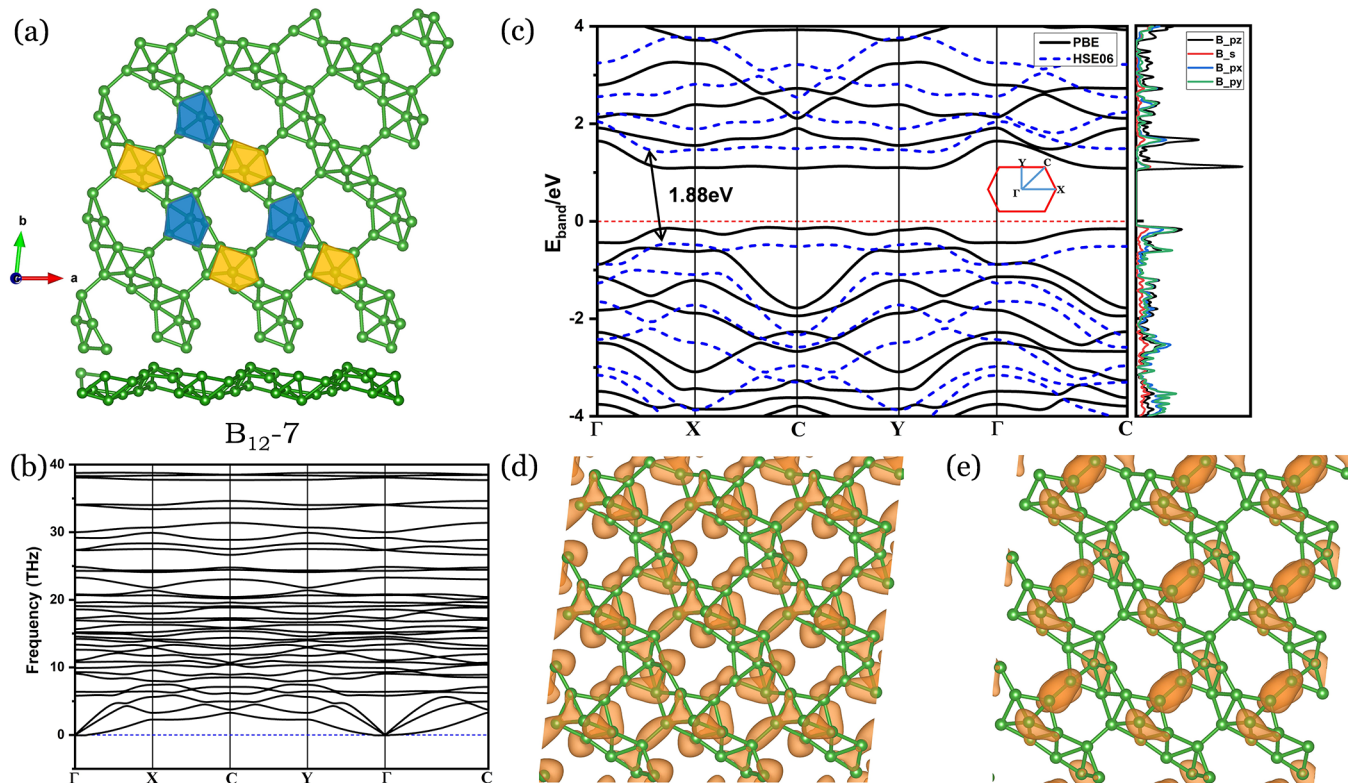


Figure 5. Atomic structure and electronic structure of semiconducting B_{12} -7 borophene with the largest bandgap. (a) Structure of B_{12} -7 borophene and basic motifs of five boron triangles. (b) Phonon spectrum of B_{12} -7 borophene. (c) Band structure and orbital-resolved DOS of B_{12} -7 borophene. Partial charge densities of (d) the VBM and (e) the CBM of B_{12} -7 borophene.

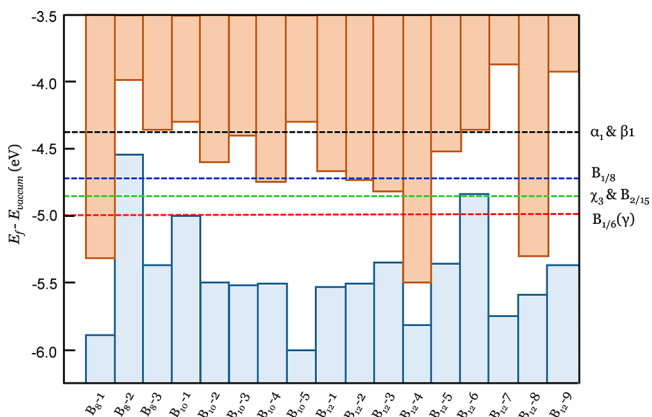


Figure 6. Fermi level positions of selected metallic borophenes denoted as a dotted line with respect to the vacuum level. The VBM and CBM positions of 17 stable semiconductor borophenes designed by IM²ODE are also shown. Blue blocks are for the VBMs and orange blocks are for the CBMs.

can also be made in this way, such as B_8 -3, B_{10} -1, B_{10} -2, B_{10} -3, and B_{10} -4, as seen in Figure 4. The B_8 -3 and B_{10} -1 structures can be seen as removing two boron atoms in the 10-boron-atom triangle lattice and buckling the atomic plane to get stabilized (Figures 4a,b). The B_{10} -2 structure (Figure 4c) is another vacancy-free polymorph of borophene with the triangle lattice, which is similar to acw-borophene and provides another example of the advantages of our searching algorithms. The B_{10} -3 structure (Figure 4d) can be seen as connected nanoribbons of triangle-lattice borophene and the B_{10} -4 (Figure 4e) structure is similar to B_{12} -1 and B_{12} -2. These

semiconducting borophenes all have indirect band gaps, as seen in the Supporting Information.

Besides the energetic stabilities, we find that our identified semiconducting borophenes can cover band gap values of a large range from 0.3 to 1.9 eV, among which B_{12} -7 has the largest band gap of 1.88 eV. The structure of B_{12} -7 borophene is shown in Figure 5a, which is a stripe-like structure with two buckled B_6 units as basic motifs. In each unit, five boron atoms form a pentagon and the sixth boron atom lies in the center. Two neighboring boron stripes are connected through hollow hexagons and octagons forming lines. The phonon spectrum in Figure 5b shows that B_{12} -7 borophene is dynamically stable. The thermodynamic stability is also confirmed by the molecular dynamic simulations in Figure S1c. Figure 5c shows the band structure of B_{12} -7 borophene calculated by PBE and HSE06 functionals. Both the VBM and the CBM are along the Γ -X line, but not in the same location, indicating the indirect band gap. Different from the arrangements in B_{12} -1 and B_{12} -2, in B_{12} -7, the p_z orbital dominates around the CBM while the p_x and p_y orbitals contribute nearly equally around the VBM. From the aspect of partial charge densities shown in Figure 5d,e, the VBM of B_{12} -7 borophene is mainly distributed near the five boron rings of the motifs and the CBM is distributed at the central boron atoms and the bonds that connect the strips.

To be good channel materials, high carrier mobility must be satisfied. Using the deformation potential approximation,⁴⁹ we estimate the mobility of the three most stable semiconducting borophenes, including B_8 -acw, B_{12} -1, and B_{12} -2. The results are provided in Supporting Information Table S2, which shows that all the three semiconducting borophene phases have carrier mobilities as high as more than $1000 \text{ cm}^2 \cdot \text{V}^{-1} \cdot \text{s}^{-1}$,

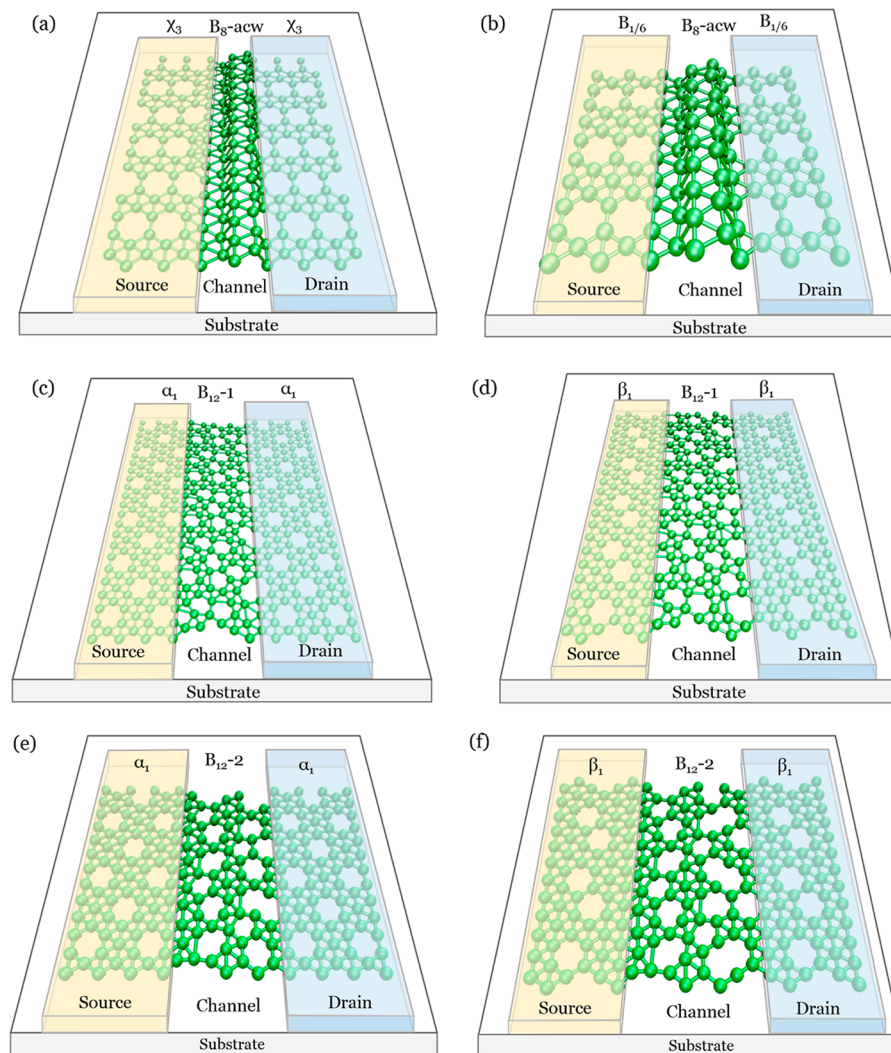


Figure 7. Schematic diagrams of 2D fully borophene-based FETs, using (a, b) B_8 -1(acw), (c, d) B_{12} -1, and (e, f) B_{12} -2 as channels. The suitable metallic borophene electrodes are also shown in corresponding diagrams.

Table 2. Proposed Lateral Junctions of Semiconducting and Metallic Borophenes with Ohmic Contacts and Negligible Lattice Mismatches

semiconductor borophenes	supercell of channel	metallic borophene electrodes	supercell of electrode	junction lattice mismatch
B_8 -1	8×1	χ_3	3×3	0.07%
	3×1	$B_{1/6}$	2×2	5%
B_{12} -1	$4\sqrt{2} \times \sqrt{2}$	α_1	5×3	0.3%
	$4\sqrt{2} \times \sqrt{2}$	β_1	5×2	0.4%
B_{12} -2	$4\sqrt{2} \times \sqrt{2}$	α_1	5×3	0.3%
	$4\sqrt{2} \times \sqrt{2}$	β_1	5×2	0.4%

demonstrating the excellent transport properties of these semiconducting borophenes as channels.

With both the metallic and semiconducting borophenes, we now turn to explore the potentials of making 2D FET using phase engineering. First, we consider the contact properties to see if Ohmic contacts between metallic electrodes and semiconducting channels can be achieved. According to a

recent theoretical work,⁵⁰ the Schottky barrier ζ in lateral metal–semiconductor junctions with sufficiently large sizes can be calculated as $\zeta_n = \varphi + \chi$ for n-type semiconducting channels and $\zeta_p = -\chi + E_g - \varphi$ for p-type semiconducting channels, where φ is the CBM position of the semiconducting channel referenced to the vacuum level, χ is the work function of metallic electrode, and E_g is the band gap of the channel. For FET applications, the smaller Schottky barriers or the Ohmic contacts with zero or negative barriers will be beneficial for the high performance. We then calculate the Schottky barriers between our identified boron semiconductors and several metallic phases, and our HSE06 results are shown in Figure 6. As we can see, $B_{1/6}$ metallic borophene can form an n-type Ohmic contact with B_8 -1, B_{12} -4, and B_{12} -8 semiconducting borophenes because the Fermi level of $B_{1/6}$ borophene is higher than those for the CBM states. Similarly, $B_{1/6}$ borophene can form p-type Ohmic contacts with B_8 -2 and B_{12} -6 borophenes. The most stable semiconducting borophene B_{12} -1, on the other hand, can only form an n-type Ohmic contact with α_1 or β_1 borophene because the CBM of B_{12} -1 is lower than the Fermi levels of α_1 and β_1 .

Next, we consider if the above-mentioned semiconducting channels and metallic borophenes with Ohmic contacts can

form sharp interfaces with negligible lattice mismatches. Because the lattices of semiconducting B_8 -1, B_{12} -1, and B_{12} -2 borophenes and all the known metallic borophenes can all been seen as derived structures from the undistorted vacancy-free boron triangle lattices, they are expected to form ideal lateral junctions by choosing the suitable superlattices, which enables us to propose fully borophene-based FET devices. Indeed, we find that a 8×1 supercell of B_8 -1 and a 3×3 supercell of χ_3 can form a lateral junction with a negligible lattice mismatch of 0.07%, as seen in the Figure 7a. Similarly, a $4\sqrt{2} \times \sqrt{2}$ supercell of B_{12} -1 or B_{12} -2 can form an ideal lateral junction with a 5×3 (5×2) supercell of α_1 (β_1), as seen in Figure 7c,d and Figure 7e,f. The lattice mismatches in the above-mentioned junctions are all less than 1% except the junction of 3×1 B_8 -1 and 2×2 $B_{1/6}$ borophenes. Our proposed fully boron-sheet-based 2D FETs with Ohmic contacts are summarized in Table 2. The stabilities of these lateral junctions are confirmed using first-principles molecular dynamics simulations, as seen in the Figure S12.

In conclusion, using multiobjective differential optimization algorithms implemented in our self-developed IM²ODE package and with the help of *first-principles* calculations, we have successfully identified 16 new semiconducting borophenes in two dimensions. Among them, the B_{12} -1 borophene is the most stable semiconducting phase, whose total energy is lower than any other known artificially built semiconducting borophenes, demonstrating the advantages of our multi-objective structure searching method. In addition, we find the band gaps of semiconducting borophenes can cover a large range from 0.3 to 1.9 eV, providing potentials for various applications. What is more, by considering not only the band alignments between our designed semiconducting borophenes and the known metallic borophenes but also the lattice matches, we have theoretically proposed several device models of fully boron-sheet-based 2D FET. Our work is expected to open up a new direction of 2D FET devices and will be helpful for the design of 2D FETs with Ohmic contacts based on phase engineering.

■ ASSOCIATED CONTENT

SI Supporting Information

The Supporting Information is available free of charge at <https://pubs.acs.org/doi/10.1021/acs.jpcllett.0c03333>.

Molecular dynamical simulation results for B_{12} -1, B_{12} -2, and B_{12} -7 borophenes at $T = 300$ K, the background and theoretical basement of IM²ODE, the atomic structure and electronic structure of B_8 -2 borophene, the phonon spectra of B_8 -2 and B_8 -3 borophenes, the atomic structure of B_{10} -5 borophene, the electronic structures of B_{10} series semiconductor borophenes, the phonon spectra of B_{10} series semiconductor borophenes, the atomic structure and electronic structure of B_{12} -3/4/5/6/8/9 borophenes, the phonon spectra of B_{12} -3/4/5/6/8/9 borophenes, molecular dynamical simulation results for B_8 -2/3 borophenes at 300 K, molecular dynamical simulation results for B_{10} series semiconductor borophenes at 300 K, molecular dynamical simulation results for B_{12} -3/4/5/6/8/9 borophenes at 300 K, estimated carrier mobilities of predicted semiconducting borophenes B8-acw/ B_{12} -1/ B_{12} -2 and molecular dynamical simulation results for 2D fully borophene-based FETs at 300 K (PDF)

■ AUTHOR INFORMATION

Corresponding Authors

Ji-Hui Yang – Key Laboratory of Computational Physical Sciences (Ministry of Education), State Key Laboratory of Surface Physics, and Department of Physics, Fudan University, Shanghai 200433, P. R. China; orcid.org/0000-0003-0642-5344; Email: jhyang04@fudan.edu.cn

Xin-Gao Gong – Key Laboratory of Computational Physical Sciences (Ministry of Education), State Key Laboratory of Surface Physics, and Department of Physics, Fudan University, Shanghai 200433, P. R. China; Collaborative Innovation Center of Advanced Microstructures, Nanjing 210093, P. R. China; Email: xggong@fudan.edu.cn

Authors

Yi-Lin Zhang – Key Laboratory of Computational Physical Sciences (Ministry of Education), State Key Laboratory of Surface Physics, and Department of Physics, Fudan University, Shanghai 200433, P. R. China; Collaborative Innovation Center of Advanced Microstructures, Nanjing 210093, P. R. China

Hongjun Xiang – Key Laboratory of Computational Physical Sciences (Ministry of Education), State Key Laboratory of Surface Physics, and Department of Physics, Fudan University, Shanghai 200433, P. R. China; Collaborative Innovation Center of Advanced Microstructures, Nanjing 210093, P. R. China; orcid.org/0000-0002-9396-3214

Complete contact information is available at:

<https://pubs.acs.org/10.1021/acs.jpcllett.0c03333>

Notes

The authors declare no competing financial interest.

■ ACKNOWLEDGMENTS

We appreciate useful discussions with Dr. Zhang Yueyu from Imperial College London and Miss Wu Na and Mr. Zhang Pan from Fudan University. This work was supported in part by the National Key Research and Development Program of China (Grant No. 2016YFB0700700), the National Natural Science Foundation of China (Grant No. 61904035), the Fudan Start-up funding (JIH1512034), and the Shanghai Sailing Program (19YF1403100). Calculations are performed at the High-Performance Computing Center of Fudan University.

■ REFERENCES

- (1) Novoselov, K. S.; Geim, A. K.; Morozov, S. V.; Jiang, D.; Zhang, Y.; Dubonos, S. V.; Grigorieva, I. V.; Firsov, A. A. Electric field effect in atomically thin carbon films. *Science* **2004**, *306*, 666–669.
- (2) Tian, B.; Zheng, X.; Kempa, T. J.; Fang, Y.; Yu, N.; Yu, G.; Huang, J.; Lieber, C. M. Coaxial silicon nanowires as solar cells and nanoelectronic power sources. *Nature* **2007**, *449*, 885–888.
- (3) Lee, J.; Kim, H.; Kahng, S. J.; Kim, G.; Son, Y. W.; Ihm, J.; Kato, H.; Wang, Z. W.; Okazaki, T.; Shinohara, H.; et al. Bandgap modulation of carbon nanotubes by encapsulated metallofullerenes. *Nature* **2002**, *415*, 1005–1008.
- (4) Ozbay, E. Plasmonics: Merging photonics and electronics at nanoscale dimensions. *Science* **2006**, *311*, 189–193.
- (5) Schuller, J. A.; Barnard, E. S.; Cai, W.; Jun, Y. C.; White, J. S.; Brongersma, M. L. Plasmonics for extreme light concentration and manipulation. *Nat. Mater.* **2010**, *9*, 193–204.
- (6) Gratzel, M. Photoelectrochemical cells. *Nature* **2001**, *414*, 338–344.
- (7) Li, G.; Shrotriya, V.; Huang, J. S.; Yao, Y.; Moriarty, T.; Emery, K.; Yang, Y. High-efficiency solution processable polymer photo-

- voltaic cells by self-organization of polymer blends. *Nat. Mater.* **2005**, *4*, 864–868.
- (8) Bock, C.; Paquet, C.; Couillard, M.; Botton, G. A.; MacDougall, B. R. Size-selected synthesis of PtRu nano-catalysts: Reaction and size control mechanism. *J. Am. Chem. Soc.* **2004**, *126*, 8028–8037.
- (9) Zheng, Y.; Jiao, Y.; Zhu, Y.; Li, L. H.; Han, Y.; Chen, Y.; Jaroniec, M.; Qiao, S. High Electrocatalytic Hydrogen Evolution Activity of an Anomalous Ruthenium Catalyst. *J. Am. Chem. Soc.* **2016**, *138*, 16174–16181.
- (10) Chhowalla, M.; Jena, D.; Zhang, H. Two-dimensional semiconductors for transistors. *Nature Reviews Materials* **2016**, *1*, 16052.
- (11) Li, L.; Yu, Y.; Ye, G. J.; Ge, Q.; Ou, X.; Wu, H.; Feng, D.; Chen, X. H.; Zhang, Y. Black phosphorus field-effect transistors. *Nat. Nanotechnol.* **2014**, *9*, 372.
- (12) Kappera, R.; Voiry, D.; Yalcin, S. E.; Branch, B.; Gupta, G.; Mohite, A. D.; Chhowalla, M. Phase-engineered low-resistance contacts for ultrathin MoS₂ transistors. *Nat. Mater.* **2014**, *13*, 1128–1134.
- (13) Yang, J.; Zhang, Y.; Yin, W.; Gong, X. G.; Yakobson, B. I.; Wei, S. Two-dimensional SiS layers with promising electronic and optoelectronic properties: theoretical prediction. *Nano Lett.* **2016**, *16*, 1110–1117.
- (14) Das, S.; Chen, H.; Penumatcha, A. V.; Appenzeller, J. High performance multilayer MoS₂ transistors with scandium contacts. *Nano Lett.* **2013**, *13*, 100–105.
- (15) Fan, Z.; Jiang, X.; Luo, J.; Jiao, L.; Huang, R.; Li, S.; Wang, L. In-plane Schottky-barrier field-effect transistors based on 1T/2H heterojunctions of transition-metal dichalcogenides. *Phys. Rev. B: Condens. Matter Mater. Phys.* **2017**, *96*, 165402.
- (16) Cho, S.; Kim, S.; Kim, J. H.; Zhao, J.; Seok, J.; Keum, D. H.; Baik, J.; Choe, D.; Chang, K. J.; Suenaga, K. Phase patterning for ohmic homojunction contact in MoTe₂. *Science* **2015**, *349*, 625–628.
- (17) Liu, Y.; Penev, E. S.; Yakobson, B. I. Probing the synthesis of two-dimensional boron by first-principles computations. *Angew. Chem., Int. Ed.* **2013**, *52*, 3156–3159.
- (18) Penev, E. S.; Bhowmick, S.; Sadrzadeh, A.; Yakobson, B. I. Polymorphism of two-dimensional boron. *Nano Lett.* **2012**, *12*, 2441–2445.
- (19) Zhang, Z.; Yang, Y.; Gao, G.; Yakobson, B. I. Two-dimensional boron monolayers mediated by metal substrates. *Angew. Chem.* **2015**, *127*, 13214–13218.
- (20) Yu, X.; Li, L.; Xu, X.; Tang, C. Prediction of two-dimensional boron sheets by particle swarm optimization algorithm. *J. Phys. Chem. C* **2012**, *116*, 20075–20079.
- (21) Li, W. L.; Jian, T.; Chen, X.; Chen, T. T.; Lopez, G. V.; Li, J.; Wang, L. S. The planar CoB18- cluster as a motif for metalloborophenes. *Angew. Chem.* **2016**, *128*, 7484–7489.
- (22) Kong, X.; Liu, Q.; Zhang, C.; Peng, Z.; Chen, Q. Elemental two-dimensional nanosheets beyond graphene. *Chem. Soc. Rev.* **2017**, *46*, 2127–2157.
- (23) Xie, S. Y.; Wang, Y.; Li, X. B. Flat Boron: A New Cousin of Graphene. *Adv. Mater.* **2019**, *31*, 1900392.
- (24) Zhou, X.; Oganov, A. R.; Wang, Z.; Popov, I. A.; Boldyrev, A. I.; Wang, H. Two-dimensional magnetic boron. *Phys. Rev. B: Condens. Matter Mater. Phys.* **2016**, *93*, 85406.
- (25) James, A. L.; Khandelwal, S.; Dutta, A.; Jasuja, K. Boron based nanosheets as reducing templates in aqueous solutions: towards novel nanohybrids with gold nanoparticles and graphene. *Nanoscale* **2018**, *10*, 20514–20518.
- (26) Zhang, Z.; Penev, E. S.; Yakobson, B. I. Two-dimensional boron: structures, properties and applications. *Chem. Soc. Rev.* **2017**, *46*, 6746–6763.
- (27) Wu, X.; Dai, J.; Zhao, Y.; Zhuo, Z.; Yang, J.; Zeng, X. C. Two-dimensional boron monolayer sheets. *ACS Nano* **2012**, *6*, 7443–7453.
- (28) Zhang, Z.; Yang, Y.; Penev, E. S.; Yakobson, B. I. Elasticity, flexibility, and ideal strength of borophenes. *Adv. Funct. Mater.* **2017**, *27*, 1605059.
- (29) Liu, L.; Zhang, Z.; Liu, X.; Xuan, X.; Yakobson, B. I.; Hersam, M. C.; Guo, W. Borophene concentric superlattices via self-assembly of twin boundaries. *Nano Lett.* **2020**, *20*, 1315–1321.
- (30) Zhang, Z.; Mannix, A. J.; Liu, X.; Hu, Z.; Guisinger, N. P.; Hersam, M. C.; Yakobson, B. I. Near-equilibrium growth from borophene edges on silver. *Science advances* **2019**, *5*, No. eaax0246.
- (31) Feng, B.; Zhang, J.; Zhong, Q.; Li, W.; Li, S.; Li, H.; Cheng, P.; Meng, S.; Chen, L.; Wu, K. Experimental realization of two-dimensional boron sheets. *Nat. Chem.* **2016**, *8*, 563–568.
- (32) Mannix, A. J.; Zhou, X.; Kiraly, B.; Wood, J. D.; Alducin, D.; Myers, B. D.; Liu, X.; Fisher, B. L.; Santiago, U.; Guest, J. R. Synthesis of borophenes: Anisotropic, two-dimensional boron polymorphs. *Science* **2015**, *350*, 1513–1516.
- (33) Tai, G.; Hu, T.; Zhou, Y.; Wang, X.; Kong, J.; Zeng, T.; You, Y.; Wang, Q. Synthesis of atomically thin boron films on copper foils. *Angew. Chem.* **2015**, *127*, 15693–15697.
- (34) Shu, H.; Li, F.; Liang, P.; Chen, X. Unveiling the atomic structure and electronic properties of atomically thin boron sheets on an Ag (111) surface. *Nanoscale* **2016**, *8*, 16284–16291.
- (35) Li, W.; Chen, X.; Jian, T.; Chen, T.; Li, J.; Wang, L. From planar boron clusters to borophenes and metalloborophenes. *Nature Reviews Chemistry* **2017**, *1*, 71.
- (36) Yang, J.; Quhe, R.; Feng, S.; Zhang, Q.; Lei, M.; Lu, J. Interfacial properties of borophene contacts with two-dimensional semiconductors. *Phys. Chem. Chem. Phys.* **2017**, *19*, 23982–23989.
- (37) Xie, Z.; Meng, X.; Li, X.; Liang, W.; Huang, W.; Chen, K.; Chen, J.; Xing, C.; Qiu, M.; Zhang, B. Two-Dimensional Borophene: Properties, Fabrication, and Promising Applications. *Research* **2020**, *2020*, 2624617.
- (38) Xu, S.; Li, X.; Zhao, Y.; Liao, J.; Xu, W.; Yang, X.; Xu, H. Two-Dimensional Semiconducting Boron Monolayers. *J. Am. Chem. Soc.* **2017**, *139*, 17233–17236.
- (39) İpek, S.; Kilic, M. E.; Mogulkoc, A.; Cahangirov, S.; Durgun, E. Semiconducting defect-free polymorph of borophene: peierls distortion in two dimensions. *Phys. Rev. B: Condens. Matter Mater. Phys.* **2018**, *98*, 241408.
- (40) Hou, C.; Tai, G.; Hao, J.; Sheng, L.; Liu, B.; Wu, Z. Ultrastable Crystalline Semiconducting Hydrogenated Borophene. *Angew. Chem.* **2020**, *132*, 10911.
- (41) Hou, C.; Tai, G.; Wu, Z.; Hao, J. Borophene: Current Status, Challenges and Opportunities. *ChemPlusChem* **2020**, *85*, 2186–2196.
- (42) Zhang, Y.; Gao, W.; Chen, S.; Xiang, H.; Gong, X. Inverse design of materials by multi-objective differential evolution. *Comput. Mater. Sci.* **2015**, *98*, 51–55.
- (43) Storn, R.; Price, K. Differential evolution—a simple and efficient heuristic for global optimization over continuous spaces. *J. Global Optim.* **1997**, *11*, 341–359.
- (44) Li, Z.; Li, Z.; Cao, H.; Yang, J.; Shu, Q.; Zhang, Y.; Xiang, H. J.; Gong, X. G. What are grain boundary structures in graphene? *Nanoscale* **2014**, *6*, 4309–4315.
- (45) Kresse, G.; Hafner, J. Ab initio molecular-dynamics simulation of the liquid-metal–amorphous-semiconductor transition in germanium. *Phys. Rev. B: Condens. Matter Mater. Phys.* **1994**, *49*, 14251.
- (46) Blöchl, P. E. Projector augmented-wave method. *Phys. Rev. B: Condens. Matter Mater. Phys.* **1994**, *50*, 17953.
- (47) Perdew, J. P.; Burke, K.; Ernzerhof, M. Generalized gradient approximation made simple. *Phys. Rev. Lett.* **1996**, *77*, 3865.
- (48) Heyd, J.; Scuseria, G. E.; Ernzerhof, M. Hybrid functionals based on a screened Coulomb potential. *J. Chem. Phys.* **2003**, *118*, 8207–8215.
- (49) Bardeen, J.; Shockley, W. Deformation potentials and mobilities in non-polar crystals. *Phys. Rev.* **1950**, *80*, 72.
- (50) Zhang, J.; Xie, W.; Zhao, J.; Zhang, S. Band alignment of two-dimensional lateral heterostructures. *2D Mater.* **2017**, *4*, 015038.